

Evolution of primordial magnetic fields from phase transitionsTina Kahniashvili,^{1,2,3,*} Alexander G. Tevzadze,^{4,†} Axel Brandenburg,^{5,6,‡} and Andrii Neronov^{7,8,§}¹*McWilliams Center for Cosmology and Department of Physics, Carnegie Mellon University, 5000 Forbes Avenue, Pittsburgh, Pennsylvania 15213, USA*²*Department of Physics, Laurentian University, Ramsey Lake Road, Sudbury, Ontario P3E 2C6, Canada*³*Abastumani Astrophysical Observatory, Ilia State University, 3-5 Cholokashvili Avenue, Tbilisi 0160, Georgia*⁴*Faculty of Exact and Natural Sciences, Tbilisi State University, 1 Chavchavadze Avenue, Tbilisi 0128, Georgia*⁵*Nordita, KTH Royal Institute of Technology and Stockholm University, Roslagstullsbacken 23, 10691 Stockholm, Sweden*⁶*Department of Astronomy, Stockholm University, 10691 Stockholm, Sweden*⁷*ISDC Data Centre for Astrophysics, Chemin d'Ecogia 16, 1290 Versoix, Switzerland*⁸*Geneva Observatory, Chemin des Maillettes 51, 1290 Sauverny, Switzerland*

(Received 10 December 2012; published 18 April 2013)

We consider the evolution of primordial magnetic fields generated during cosmological, electroweak, or QCD phase transitions. We assume that the magnetic field generation can be described as an injection of magnetic energy to cosmological plasma at a given scale determined by the moment of magnetic field generation. A high Reynolds number ensures strong coupling between the magnetic field and fluid motions. The subsequent evolution of the magnetic field is governed by decaying hydromagnetic turbulence. Both our numerical simulations and a phenomenological description allow us to recover “universal” laws for the decay of magnetic energy and the growth of magnetic correlation length in the turbulent (low-viscosity) regime. In particular, we show that during the radiation-dominated epoch, the energy and correlation length of nonhelical magnetic fields scale as conformal time to the powers $-1/2$ and $+1/2$, respectively. For helical magnetic fields, the energy and correlation length scale as conformal time to the powers $-1/3$ and $+2/3$, respectively. The universal decay law of the magnetic field implies that the strength of the magnetic field generated during the QCD phase transition could reach $\sim 10^{-9}$ G with the present-day correlation length ~ 50 kpc. The fields generated at the electroweak phase transition could be as strong as $\sim 10^{-10}$ G with correlation lengths reaching ~ 0.3 kpc. These values of the magnetic fields are consistent with the lower bounds of the extragalactic magnetic fields.

DOI: [10.1103/PhysRevD.87.083007](https://doi.org/10.1103/PhysRevD.87.083007)

PACS numbers: 98.70.Vc, 98.80.-k

I. INTRODUCTION

Astronomical observations show that galaxies have magnetic fields with a component that is coherent over a large fraction of the galaxy with field strengths of the order of 10^{-6} G; see Refs. [1–3] and references therein. Understanding the origin of these fields is one of the challenging questions of modern astrophysics. Generally speaking, there are two popular scenarios. The first one envisages the generation of magnetic fields through different astrophysical mechanisms. More precisely, it is assumed that an initially tiny magnetic field is produced through a battery mechanism [4]. The correlation length of such a field is limited by galactic length scales. The second scenario to explain the origin of the magnetic field in galaxies and clusters presumes that the observed magnetic fields were amplified from cosmological weak seed magnetic fields [5]. In this case the correlation length of such a seed field might be as large as the horizon scale today if we admit that the field has been generated during

inflation. There are different possibilities for seed magnetic field amplification, ranging from a magnetohydrodynamic (MHD) dynamo to the adiabatic compression of magnetic field lines during structure formation [6,7].

Galactic magnetic fields are usually measured through the induced Faraday rotation effect [2,3] and, as mentioned above, the field magnitude is of the order of a few 10^{-6} G at typical scales of 10 kpc. The primordial magnetic energy density contributes to the radiation field, and thus the big bang nucleosynthesis (BBN) bound implies $\Omega_B h_0^2 \leq 2.4 \times 10^{-6}$ [8] if the magnetic field has been generated prior to BBN. If the correlation length of the magnetic field is much larger than $\lambda_B \geq 1$ Mpc, smaller limits on the magnetic field energy density arise from the cosmological data, making $B_{\max} \leq$ a few 10^{-9} G; see Ref. [9] and references therein. A correlation length-dependent lower limit on magnetic fields in the intergalactic medium (IGM) could be derived from gamma-ray observations of blazars [10–13]. In the limit of large correlation lengths, $\lambda_B \geq 1$ Mpc, the bound is at the level of 10^{-17} G (see also Ref. [14] for a discussion on possible uncertainties in the measurements of blazar spectra).

It is possible, in principle, that the IGM magnetic fields are of primordial origin. Another possibility is that the

*tinatin@phys.ksu.edu

†aleko@tevza.org

‡brandenb@nordita.org

§Andrii.Neronov@unige.ch

fields are spread through the IGM by outflows from galaxies at late stages of the evolution of the Universe. To distinguish between these two possibilities, it is important to identify measurable characteristics of the IGM magnetic fields which are different in the two cases and to study the possibility of measuring such characteristics.

In this paper we consider the observational properties of IGM magnetic fields expected if the fields originate from cosmological phase transitions (PT) such as the electroweak (EW) and QCD PTs [15,16]. Some scenarios of magnetic field generation during electro weak phase transition (EWPT) or QCDPT also produce magnetic helicity [17]. We follow the evolution of fields from the epoch right after the magnetogenesis up to the present-day epoch. Our approach is different from that adopted in the previous studies, which mostly concentrated on the analysis of the range of possible field strengths at a predefined scale of interest (e.g., 1 Mpc). Instead, we study the evolution of field characteristics that are most relevant for measurements using radio and gamma-ray astronomy. Specifically, we are interested in the evolution of the magnetic energy density ρ_B , which determines the characteristic field strength $B^{(\text{eff})} = \sqrt{8\pi\rho_B}$, and the characteristic correlation scale (integral scale) λ_M at which the field reaches the strength $B^{(\text{eff})}$.

The present-day integral scale depends on the temperature T_* and the number of relativistic degrees of freedom g_* at the moment when the primordial magnetic field is generated. These parameters determine the maximal allowed value of the magnetic energy density injected in the PT plasma, as well as the initial correlation length of the magnetic field [18]. We do not separately consider the effect of helicity transfer related to the chiral anomaly, which might be important in the presence of strong magnetic fields at temperatures above 10–100 MeV [19]. Such a transfer could be considered as part of the magnetogenesis process which could persist all the way down to the temperature scale of the QCD phase transition. We only use fundamental physical laws, such as conservation of energy, and the way the magnetic field interacts with the cosmological plasma through MHD turbulence, and we do not make any assumption about the physical processes responsible for the primordial magnetic field generation.

In Sec. II we give an overview of the spatial and temporal characteristics of the primordial magnetic field. The results of our analysis are presented in Sec. III, where we discuss the evolution of the magnetic field. Conclusions are presented in Sec. IV. We employ natural units with $\hbar = 1 = c$ and Gaussian units for electromagnetic quantities.

II. MODEL DESCRIPTION

A. Effective magnetic field characteristics

We assume that the phase-transition-generated magnetic fields satisfy the causality condition [16,20,21]. The maximal correlation length ξ_{max} for a causally generated

primordial magnetic field cannot exceed the Hubble radius at the time of generation, H_*^{-1} . Hence $\gamma = \xi_{\text{max}}/H_*^{-1} \leq 1$, where γ can be associated with the number of primordial magnetic field bubbles within the Hubble radius, $N \propto \gamma^3$. The comoving length (measured today) corresponding to the Hubble radius at generation is inversely proportional to the corresponding PT temperature T_* ,

$$\lambda_{H_*} = 5.8 \times 10^{-10} \text{ Mpc} \left(\frac{100 \text{ GeV}}{T_*} \right) \left(\frac{100}{g_*} \right)^{1/6}, \quad (1)$$

and is equal to 0.5 pc for the QCDPT (with $g_* = 15$ and $T_* = 0.15 \text{ GeV}$) and 6×10^{-4} pc for the EWPT (with $g_* = 100$ and $T_* = 100 \text{ GeV}$), and the comoving primordial magnetic field correlation length $\xi_{\text{max}} \leq \lambda_H$. This inequality assumes *only* the expansion of the Universe, without accounting for MHD turbulence (free turbulence decay or an inverse cascade if a helical primordial magnetic field is present). We also note that the number of PT bubbles within the Hubble radius is around 6 ($\gamma \simeq 0.15$) for QCDPT and around 100 ($\gamma \simeq 0.01$) for EWPT. So the maximal correlation length ξ_{max} is equal to 0.08 pc for QCDPT and 6×10^{-6} pc for EWPT.

The maximal value of the primordial magnetic field energy density must satisfy the BBN bound, i.e., the total energy density of the primordial magnetic field at nucleosynthesis ρ_B [where a should not exceed 10% of the radiation energy density $\rho_{\text{rad}}(a_N)$]. In any case, the magnetic field is generated by the mechanical motion of charged particles, so its energy density could constitute only a fraction of the matter energy density, which is at most comparable to the radiation energy density in the radiation-dominated Universe. Note that the maximal value of the effective magnetic field is independent of the temperature at generation T_* , and depends only very weakly on the number of relativistic degrees of freedom at the moment of generation.

In what follows, we are mostly interested in the evolution of the energy density of the magnetic field and the length scale which gives the dominant contribution to the energy density (the “integral scale”) during the course of cosmological evolution. Taking this into account, we adopt the following idealizing approximation: We generate an initial primordial magnetic field by solving the MHD equations for a certain time during which an external electromagnetic force is applied that is proportional to a delta function that peaks at the characteristic scale $k_0 = 2\pi/\xi_0^{-1}$. This corresponds to a magnetic field with correlation length ξ_0 . In this approximation, the characteristic magnetic field strength at the scale ξ_0 is $B^{(\text{eff})} = \sqrt{8\pi\rho_B}$. We justify our assumption that ξ_0 should be identified with the size of the largest magnetic eddies by noting that the primordial magnetic field is involved in MHD processes driven by turbulence. It is natural to assume that the typical length scale of the magnetic field generated during the PTs is determined by the PT bubble size.

The dynamical evolution of the coupled magnetic field—matter system leads to a spread of magnetic field over a range of scales. The resulting power spectrum of the magnetic field at small wave numbers (or, equivalently, large distance scales) has the form of a power law, $P_M(k) = E_M(k)/(4\pi k^2) = Ak^{n_B}$, with a normalization constant A and a slope¹ n_B . In particular, a white noise power spectrum corresponds to $n_B = 0$ [20], while the Batchelor spectrum corresponds to $n_B = 2$ [21]. The power-law spectrum extends up to a time-dependent integral scale ξ_M , above which the power contained in the magnetic field decreases rapidly due to turbulent decay and/or viscosity damping.

Several previous studies (see Ref. [23] and references therein) describe the primordial magnetic field in terms of a smoothed (over length scale ξ) magnetic field B_ξ with $B_\xi^2 = \langle B_i(\mathbf{x})B_i(\mathbf{x}) \rangle|_\xi$. Knowing $B^{(\text{eff})}$ and the slope of the power spectrum, one can calculate the strength of the smoothed magnetic field at any scale of interest ξ [18]:

$$B_\xi = \frac{B^{(\text{eff})} \sqrt{\Gamma(n_B/2 + 5/2)}}{(\xi/\xi_M)^{(n_B+3)/2}}. \quad (3)$$

The smoothed magnetic field might be of interest in the context of certain problems. For example, the strength of a magnetic field smoothed over a scale $\xi \sim 1$ Mpc is considered to be relevant in the context of seed magnetic fields for galactic dynamos. It is, however, important to note that B_ξ is strongly n_B dependent for a given value of ξ . In particular, for causally generated magnetic fields with $n_B \geq 0$ there is significant “magnetic power” only at small scales, and for $\xi \simeq 1$ Mpc the value of $B_{1 \text{ Mpc}}$ is extremely small [24]. At the same time, it does not imply that the magnetic field itself is weak. In fact, it could be as strong as $B^{(\text{eff})} \simeq 10^{-6} - 10^{-7}$ G, close to the bound imposed by the BBN [18]. Only in the case of a scale-invariant magnetic field with $n_B \rightarrow -3$, generated, for example, during inflation [25], B_ξ is independent of ξ and n_B , and is equal to $B^{(\text{eff})}$. Note that sometimes [see, e.g., Eq. (8) in Ref. [26]], instead of calculating B_ξ through $B^{(\text{eff})}$, the smoothed value of the magnetic field is determined through the normalization constant A of the power spectrum as $B_\xi^2 = A\Gamma(n_B/2 + 3/2)/(\xi_M)^{(n_B+3)}/(2\pi)^2$.

¹In general, the magnetic field spectrum is determined through the Fourier transform $F_{ij}^M(\mathbf{k})$ of the two-point correlation function of the magnetic field, $\langle B_i(\mathbf{x})B_j(\mathbf{x} + \mathbf{r}) \rangle$, with the spectral function [22]

$$F_{ij}^M(\mathbf{k}) = P_{ij}(\mathbf{k}) \frac{E^M(k)}{4\pi k^2} + i\varepsilon_{ijl}k_l \frac{H^M(k)}{8\pi k^2}. \quad (2)$$

Here, $P_{ij}(\mathbf{k}) = \delta_{ij} - k_i k_j / k^2$, ε_{ijl} is the antisymmetric tensor, and $E^M(k)$ and $H^M(k)$ are the magnetic energy and helicity spectra.

B. Phenomenological description of the magnetic field decay in the free turbulence regime

After generation, the evolution of the primordial magnetic field is a complex process affected by MHD as well as by the expansion of the Universe [27–35]. In our description, to account for the expansion of the Universe we make use of the fact that conformal invariance allows for a description of MHD processes in the early Universe by simply rescaling all physical quantities in terms of their comoving values and using the conformal time η [16]. After this procedure, the MHD equations include the effects of the expansion while retaining their conventional flat spacetime form.

The magnetic evolution process strongly depends on initial conditions, as well as on the physical conditions of the primordial plasma. We need to determine the scaling laws for the following magnetic field characteristics: (i) magnetic energy density, (ii) correlation length, and (iii) magnetic helicity. The magnetic energy and magnetic helicity spectra are related through the realizability condition, $|H_M(k, \eta)| \leq 2E_M(k, \eta)/k$ [29]. For the total magnetic energy $\mathcal{E}_M(t) = \int E_M(k, \eta) dk$ and helicity $\mathcal{H}_M(\eta) = \int H_M(k, \eta) dk$, we get

$$\mathcal{H}_M(\eta) \leq 2\xi_M(\eta)\mathcal{E}_M(\eta), \quad (4)$$

where

$$\xi_M(\eta) \equiv \mathcal{E}_M^{-1}(\eta) \int E_M(k, \eta) k^{-1} dk \quad (5)$$

is the comoving magnetic eddy correlation length (which corresponds to the physical integral scale λ_M), initially set by the temperature at the magnetic field generation moment $\xi_{M,\text{in}} = \lambda_0 = \gamma\lambda_{H_*}$ [see Eq. (1)], and is independent of the presence of magnetic helicity.

Both helical and nonhelical magnetic fields experience large-scale MHD decay, resulting in an increase of the correlation length with a corresponding decrease in the magnetic energy density at large scales; for a review, see Refs. [29,36]. The time rate of this process depends strongly on the presence of magnetic helicity [27,28]. Taking this into account, we consider the cases of helical and nonhelical magnetic fields separately.

As noted above, the initial magnetic field configuration is given by a sharply peaked spectral energy density. The coupling between the primordial magnetic field and plasma, which ensures the spreading of the fixed-scale primordial magnetic field over a wide range of length scales, forms a modified magnetic field spectrum within a few turnover times (see Ref. [37] for more details). The final realization of the spectrum is given by the Batchelor spectrum, $n_B = 2$. Our numerical simulation results are in perfect agreement with the “causality constraint” that in the cosmological context has been discussed in Ref. [16]

and studied through an analytical approach in Ref. [21],² so that the power contained in the large-scale modes is very small, while the total magnetic energy density is sufficiently large. MHD processes are also responsible for the generation of fluid perturbations when an initial magnetic field is present. These processes finally result in equipartition between magnetic and kinetic energy densities [34,39]. In contrast to the magnetic field, the velocity field has a white noise spectrum, i.e., $P_K = E_K/(4\pi k^2) = A_K k^{n_K}$, with $n_K = 0$ due to the possible presence of longitudinal modes. To describe adequately the evolution of fluid motions coupled to the magnetic field, we need to solve the complete set of MHD equations; see below.

Below we present a phenomenological description of the MHD decay laws at large scales. In the case of helical fields, we mostly follow the description presented in Secs. 4.2.3 and 5.3.2 of Ref. [29] and Sec. 7.3.4 of Ref. [40]. On scales below ξ_M , magnetic power is transferred to smaller scales via the so-called *direct cascade* by turbulence until it is finally damped at the smallest scale ξ_d . In MHD, the magnetic field damping is usually determined through the Reynolds number as $\xi_d/\xi_M = \text{Re}^{-3/4}$ [36]. The kinetic and magnetic Reynolds numbers in the early Universe can be extremely high, and thus one may expect that $\xi_d \ll \xi_M$. In both helical and nonhelical cases, the dissipative region of the energy density spectrum is given by a Kolmogorov-type spectrum³ $E_M = C_K \varepsilon_M^{2/3} k^{-5/3}$, where C_K is a constant of order unity (1.6–1.7 for a wide range of Reynolds numbers), ε_M is the magnetic energy dissipation rate per unit mass, given by $\varepsilon_M = 2\lambda \int_{k_0}^{k_D} k^2 E_M(k)$, with λ being the magnetic diffusivity. At large scales above ξ_M , the magnetic field decay is strongly dependent on the presence of magnetic helicity. The high conductivity of plasma ensures magnetic helicity conservation that is responsible for the transfer of spectral energy from small to large scales via a so-called *inverse cascade*. In the nonhelical case, the process is more complicated. As we will see below, magnetic helicity conservation leads to a faster growth of the correlation length and a slower decay of total magnetic energy.

²A recent study based on semianalytical calculations [38] showed the same shape for phase-transition-generated magnetic fields. In laboratory plasma as well as in numerical simulations, the resulting magnetic field spectrum at large scales can be given by a white noise spectrum, $n_B = 0$ [20], or even by a flatter Kazantsev spectrum, $n_B = -1/2$ [29]. However, here we consider the case of a cosmological magnetic field for which the correlation length is strongly limited by the Hubble horizon.

³By a Kolmogorov-type spectrum, we simply mean a $k^{-5/3}$ spectrum, ignoring anisotropies that are known to exist in nonhelical MHD [41]. Such a spectrum can be derived from a phenomenological approach too; see Sec. 5.3.2. of Ref. [29]. Our numerical simulations [37,42] confirmed the Kolmogorov-type spectrum for a wide range of magnetic Prandtl numbers.

1. Nonhelical magnetic fields

As we already stated above, causality requires that $E_M(k) \propto k^4$, and this is a consequence of the divergence-free condition for the magnetic field [21]. On the other hand, there is no zero-divergence requirement for the velocity field, and this allows for the possibility of having a white noise spectrum for the velocity field, i.e., $E_K(k) \propto k^2$; see Ref. [20]. We would like to note that our numerical simulations allowing the longitudinal forcing (see Refs. [34,39]) show a white noise spectrum for the velocity field as a final configuration. Under these conditions, the power of magnetic field modes on the large scales is much smaller than the power of plasma motions. Thus, potentially the magnetic field might be amplified via a transfer of energy from plasma motions at large scales. The time scale η on which the field can be amplified at large scales can be deduced from the induction equation

$$\frac{\partial B}{\partial t} \sim \frac{v_K(L)B}{L} \rightarrow \eta \sim L/v_L, \quad (6)$$

i.e., the characteristic field amplification time scale is approximately the plasma eddy turnover time. On this time scale, an equipartition between kinetic and magnetic energies could be reached over the distance range L . In the final configuration the equipartition between magnetic and kinetic energies is a consequence of the coupling between magnetic and velocity fields.⁴ The growth of the magnetic field up to equipartition with the fluid on large scales is somewhat similar to the phenomenon of an “inverse cascade” of the magnetic power spectrum. Note, however, that the source of power in the inverse transfer of nonhelical magnetic fields is different from the power source in the case of helical fields. In the case of nonhelical fields, the power in the large-wavelength modes increases due to the presence of a large power reservoir in the form of the turbulent motions of the plasma in the same wavelength range. By contrast, in the case of helical fields, the power on large scales grows due to the transfer of power from the shorter-wavelength modes.

Apart from the transfer of power from the plasma motions to the magnetic field at large scales, another effect of the evolution of plasma and magnetic field perturbations is the turbulent decay of the power at short length scales due to the phenomenon of the direct turbulent cascade. At a given moment of time η , this phenomenon leads to the

⁴In fact, the two Reynolds numbers in the Universe are high enough to ensure the validity of the Kolmogorov-type phenomenological approach [30], according to which there is self-similarity between the kinetic and magnetic energy densities’ evolution (see Sec. 7.3.4 of Ref. [40]), i.e.,

$$\mathcal{E}_M \sim \mathcal{E}_K \sim \mathcal{E}. \quad (7)$$

suppression of power in velocity and magnetic field modes on scales smaller than the size of the largest processed eddy. The size of the largest processed eddy is determined by the condition

$$\xi_K \sim \xi_M \sim v_K(\xi_K)\eta, \quad (8)$$

where $v_L(\xi)$ is the characteristic velocity of the plasma motions on the scale ξ . From the definition of the kinetic energy power spectrum through the velocity two-point correlation $P_K(\mathbf{k}) \sim |v_k|^2 \sim |v_K(L \sim 1/k)|^2/k^2$, one finds that the characteristic velocity v_K on the distance scale $L \sim k^{-1}$ is $v_K^2 \sim k^2 P_K$. Since the power spectrum of plasma perturbations is $P_K \sim k^0$, we have $v_K \sim k \sim \xi^{-1}$, so the above equation has the solution

$$\xi_K \sim \xi_M \sim \eta^{1/2}. \quad (9)$$

The energy of plasma perturbations on the scale ξ_K is $E_K = 4\pi k^2 P_K \sim k^2 \sim \xi_K^{-2} \sim \eta^{-1}$. Since the magnetic field on the scale $\xi_K \sim \xi_M$ is in equipartition with the plasma, the energy density of the magnetic field evolves with time as

$$E_M \sim E_K \sim \eta^{-1}, \quad (10)$$

so that the strength of magnetic field evolves as

$$B^{(\text{eff})} \sim \sqrt{E_M} \sim \eta^{-1/2}. \quad (11)$$

Below, we demonstrate numerically (see Sec. III) that the evolution laws $\xi_M \sim \eta^{1/2}$, $E_M \sim \eta^{-1}$ are indeed realized in the free turbulence decay regime. It should be noted that the ‘‘universality’’ of the decay law $\xi_M \propto \eta^{1/2}$ would not be realized if we were to consider the magnetic field evolution separately from the velocity field evolution [29]; see also Refs. [32,33] for the magnetic field decay laws in the cosmological context. Accounting for the Loitsianskii invariant for turbulence leads to the decay laws being dependent on the spectral shape; see Ref. [43] and references therein. It has also been claimed that the decay laws in the case of nonhelical magnetic fields strongly depend on the initial conditions and can be different even when the helicity is extremely small [29].

2. Helical fields

In the case of helical fields, the evolution of E_M and ξ_M is determined directly by the condition of the conservation of magnetic helicity, $\int \mathbf{A} \cdot \mathbf{B} d^3x$. High Reynolds numbers allow us to follow the Kolmogorov-type phenomenological approach given above; see Sec. 4.2.3 of Ref. [29]. Accounting for magnetic helicity conservation $\mathcal{E}_M \xi_M = \text{const.}$ ⁵ and combining Eq. (7) and $\xi_M \sim \mathcal{E}^{3/2}/\varepsilon$, which follows from the dimensionless analysis (based on the Kolmogorov-type approach), we get [30]

⁵Accounting for magnetic helicity conservation and assuming that the magnetic spectral energy is sharply peaked at ξ_M , a very rough estimate implies that $B^{\text{eff}} \propto \xi_M^{-1/2}$.

$$-\frac{d\mathcal{E}_M}{d\eta} \sim \mathcal{E}_M^{-5/2}, \quad (12)$$

which leads to the decay laws $\mathcal{E}_M \propto \eta^{-2/3}$ and $\xi_M \propto \eta^{2/3}$. Below, we demonstrate numerically (see Sec. III B) the appearance of the $\xi_M \sim t^{2/3}$, $E_M \sim t^{-2/3}$ laws in the evolution of helical magnetic fields in the free decay regime.

C. Simulation setup

To model the evolution of the magnetic field and fluid perturbations, we solve the compressible equations with the pressure given by $p = \rho c_s^2$, where ρ is the gas density and $c_s = 1/\sqrt{3}$ is the sound speed for an ultrarelativistic gas. Following our earlier work [34], we solve the governing equations for the logarithmic density $\ln \rho$, the velocity \mathbf{v} , and the magnetic vector potential \mathbf{A} , in the form

$$\frac{D \ln \rho}{D\eta} = -\nabla \cdot \mathbf{v}, \quad (13)$$

$$\frac{\mathbf{v}}{\eta} = \frac{\mathbf{J} \times \mathbf{B}}{\rho} - c_s^2 \nabla \ln \rho + \mathbf{f}_{\text{visc}} \quad (14)$$

$$\frac{\partial \mathbf{A}}{\partial \eta} = \mathbf{v} \times \mathbf{B} + \mathbf{f}_M + \lambda \nabla^2 \mathbf{A}, \quad (15)$$

where $D/D\eta = \partial/\partial\eta + \mathbf{v} \cdot \nabla$ is the advective derivative and $\mathbf{f}_{\text{visc}} = \nu(\nabla^2 \mathbf{v} + \frac{1}{3} \nabla \nabla \cdot \mathbf{v} + \mathbf{G})$ is the viscous force in the compressible case, with constant kinematic viscosity ν and $G_i = 2\mathbf{S}_{ij} \nabla_j \ln \rho$, as well as $\mathbf{S}_{ij} = \frac{1}{2}(\mathbf{v}_{i,j} + \mathbf{v}_{j,i}) - \frac{1}{3} \delta_{ij} \mathbf{v}_{k,k}$, which is the trace-free rate-of-strain tensor. Furthermore, $\mathbf{J} = \nabla \times \mathbf{B}/4\pi$ is the current density.

We use the PENCIL CODE [44] with a resolution of 512^3 meshpoints. An important difference between our simulation setup and those of previous studies is in the treatment of the backreaction of fluid perturbations onto the magnetic field. Such treatment is important, especially on large length scales, because the spectrum of velocity perturbations follows a white noise ($E_K \propto k^2$) spectrum to large scales [20]. Large-scale fluid perturbations affect the magnetic field evolution at the largest scales and could lead to a transfer of power to the large-scale modes of the magnetic field, an effect similar to the inverse cascade developing even in the case of nonhelical fields; see also Sec. III.

Prior to the simulation of the magnetic field decay, we inject magnetic energy into the computational domain at scales corresponding to the phase-transition eddy size (see Ref. [34] for more details). We approximate the magnetic field injection by a delta function in wave number space, allowing it to interact through MHD processes with a rest plasma. After several turnover times, the initial sharp peak of the magnetic field starts to disappear and the magnetic field begins to spread over a wide range of the wave numbers; see Fig. 4 of Ref. [34]. In a few turnover times, the spectrum becomes established with a cutoff at small length scales and a well-defined Kolmogorov-like integral

scale k_M , and a k^4 spectral shape at large length scales. In contrast to the studies of Refs. [32,33], we recover the spectral shape of the magnetic field at large scales.⁶ This is in perfect agreement with the previous analytical results of Ref. [21] based on causality and divergence-free field arguments.

We use simple power-law models for the decay of turbulence and scale the magnetic correlation length and magnetic field with temperature as follows:

$$\frac{\xi_M}{\lambda_0} = \left(\frac{T}{T_*}\right)^{-n_\xi}, \quad (16)$$

$$\frac{B^{(\text{eff})}}{B_*} = \left(\frac{T}{T_*}\right)^{-n_E}, \quad (17)$$

where B_* and T_* are the effective values of the magnetic field at the moment of generation and the temperature of the phase transition, respectively. Hence, the values of the parameters n_ξ and n_E describe the turbulent decay laws that differ from each other in the nonhelical and helical cases.

Qualitative arguments presented above show that the expected values for (n_ξ, n_E) for nonhelical and helical fields are $(1/2, -1/2)$ and $(2/3, -1/3)$, respectively. Below, we show that this is indeed the case.

III. SIMULATION RESULTS

In Sec. II, we have presented a phenomenological description of the scaling laws for the magnetic correlation length and the magnetic energy in the free turbulence decay regime. Below, we address the same scaling laws based on our simulations. We also briefly review the results of previous works.

A. Nonhelical magnetic field evolution

The scaling laws for the nonhelical magnetic field evolution have been studied through different simulations by different groups; see Refs. [27,28,30,32,45] and references therein. As is stated in Ref. [29], the magnetic decay laws for the nonhelical case strongly depend on initial conditions, and result in exponents n in the decay law $\mathcal{E}_M(\eta) \propto \eta^{-n}$ that vary in the range $1.3 > n > 0.65$. Note that the numerical and phenomenological studies performed in Refs. [32,33] lead to $\xi_M(\eta) \propto \eta^{0.4}$ and $\mathcal{E}_M(\eta) \propto \eta^{-1.2}$ for a white noise spectrum, and this is in good agreement with the grid turbulence description of hydrodynamic turbulence [36]. On the other hand, the 3D MHD simulations of Refs. [27,34] and the phenomenological study of Ref. [31] show a slightly faster growth of the correlation length $\xi_M(\eta) \propto \eta^{1/2}$ with a magnetic energy decaying as $\mathcal{E}_M \propto t^{-1}$. The difference between the two different scaling

⁶Note that in Ref. [34], the spectral index is between 3 and 4 due to a different choice of the system parameters and run time.

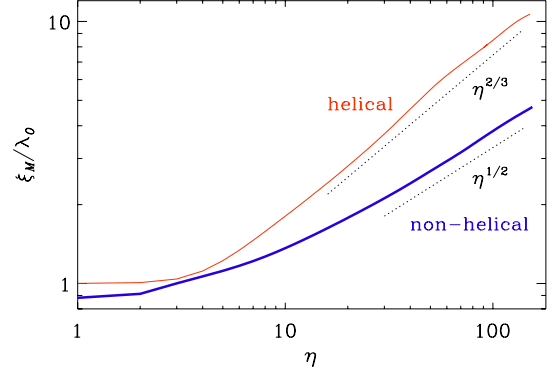


FIG. 1 (color online). $\xi_M(\xi)$ for helical (thin, red) and non-helical (thick, blue) cases.

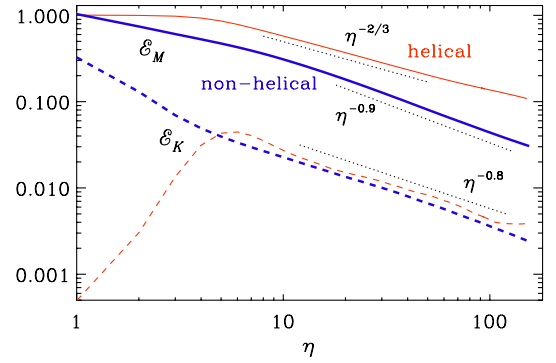


FIG. 2 (color online). $\mathcal{E}_M(\xi)$ (solid) and $\mathcal{E}_K(\xi)$ (dashed) for the helical (thin, red) and nonhelical (thick, blue) cases.

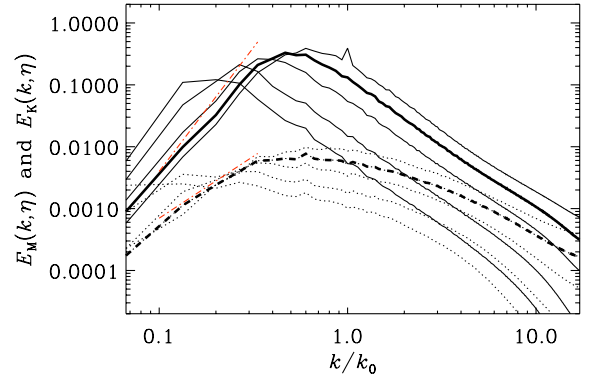


FIG. 3 (color online). Evolution of $E_M(k, \xi)$ (solid) and $E_K(k, \xi)$ (dashed) versus k for $\eta = 5, 10, 20, 50,$ and 100 for the nonhelical run. Thick lines are for $\eta = 10$. The red dash-dotted lines give the k^2 and k^4 scalings for comparison. All spectra are normalized by $\int E_M(k, 0) dk/k_0$.

laws is probably due to different initial conditions. In particular, the initial velocity field has traditionally been taken to be zero. By contrast, here we have taken as initial condition the result of a self-consistent magnetically driven turbulence simulation. The numerical simulations of Ref. [42] show that the growth of the correlation length

is almost independent of the magnetic Prandtl number with $\xi_M \propto \eta^{1/2}$ (Fig. 1), while the exponent of the total magnetic energy density decay is compatible with -1 (here closest to -0.9 ; Fig. 2). Accounting for $T \propto a^{-1}$ and $\propto \eta^{-1}$ during the radiation-dominated epoch, and the magnetic field strength $B^{(\text{eff})} = \sqrt{8\pi\mathcal{E}M}$, we get the scaling indices for the decay of nonhelical turbulence: $n_\xi = 1/2$ and $n_E = -1/2$. As expected, for $k \ll k_0$ early times, we find $E_M(k, \xi) \propto k^4$ and $E_K(k, \xi) \propto k^2$; see Fig. 3. Furthermore, even in this nonhelical case the spectral energies increase with time for $k \ll k_0$, while for $k \gg k_0$ they decrease.

B. Helical magnetic field evolution

As we have noted above, the presence of magnetic helicity results in the development of an inverse cascade during which the correlation length is increasing while the total magnetic energy decreases. Similar to the nonhelical case, there are basically two different approaches: (i) Refs. [30,32,33] assume exact conservation of magnetic helicity, and the magnetic field is the dominant contribution to the total energy density, i.e., $\mathcal{E}_K/\mathcal{E}_M \ll 1$ (where \mathcal{E}_K is the total kinetic energy density of turbulence); (ii) other approaches are given in Refs. [27,31]. In particular, Ref. [27] refers to a more general case with magnetic helicity evolving as $\mathcal{H}_M(\eta) \propto \eta^{-2s}$. Also, the ratio between kinetic and magnetic energy densities has in some studies been assumed to be around 1; Ref. [31] assumes that the magnetic field evolves toward a force-free regime with constant magnetic helicity and with a constant ratio between magnetic and kinetic energy densities. All models [28,30–33] show that the scaling laws are independent of the initial magnetic field spectrum. In fact, there are two main behaviors described: (i) Refs. [30,32,33] claim $\mathcal{E}_M(\eta) \propto \eta^{-2/3}$ and $\xi_M(\eta) \propto \eta^{2/3}$; (ii) Refs. [27,31] claim $\xi_M(\eta) \propto \eta^{1/2}$ with $\mathcal{E}_M(\eta) \propto \eta^{-1/2}$. In both scaling laws, $\xi_M \mathcal{E}_M \sim \text{const}$. The main difference between these two scaling laws consists in choosing the turbulence model. Refs. [27,31] assume a force-free development of the MHD turbulence decay, while Ref. [33] [see their Eq. (4)] assumes a linear dependence between vorticity and Lorentz force. Our new numerical results support the former scenario, (i). Figure 3 shows the evolution of kinetic and magnetic spectral energies. As we can see, the k^2 and k^4 laws are established at large scales for kinetic and magnetic spectral energies, respectively. We can also see the slight increase of power at large scales, even in the case of nonhelical fields.

We have performed a study of the large-scale decay of a maximally helical magnetic field under conditions similar to those in the nonhelical case, and for different magnetic Prandtl numbers as well as different values of magnetic resistivity. We have recovered the $E_M(k) \propto k^4$ spectral shape and the scaling laws as $\xi_M \propto \eta^{2/3}$ and $\mathcal{E}_M \propto \eta^{-2/3}$, so that $n_\xi = 2/3$, $n_E = -1/3$ [46]; see also

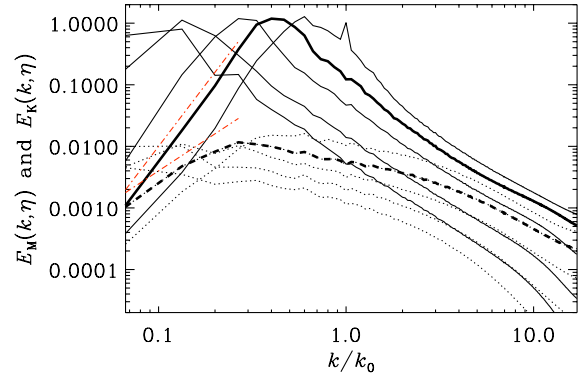


FIG. 4 (color online). Evolution of $E_M(k, \xi)$ (solid) and $E_K(k, \xi)$ (dashed) versus k for $\eta = 5, 10, 20, 50,$ and 100 for the helical run. Thick lines are for $\eta = 10$. The red dash-dotted lines give the k^2 and k^4 scalings for comparison. All spectra are normalized by $\int E_M(k, 0) dk/k_0$.

Ref. [29] for more general discussion, and see Figs. 1 and 2. Again, these scaling laws are valid when the correlation length is greater than the damping scale, so that dissipation does not play an important role. Similarly to the nonhelical run, we find for $k \ll k_0$ and early times that $E_M(k, \xi) \propto k^4$ and $E_K(k, \xi) \propto k^2$; see Fig. 4. In this case, there is a strong inverse cascade with a strong increase of spectral energies with time for $k \ll k_0$. We can also see the constant magnetic power while the peak is moving toward large scales (inverse cascade). This corresponds to the constant helicity case.

IV. IMPLICATIONS FOR THE COSMOLOGICAL EVOLUTION OF MAGNETIC FIELDS

Decay of cosmological MHD turbulence occurs together with the cooling of the Universe and the increase of magnetic correlation length. Therewith, the correlation length increases only up to the point when the Universe reaches the temperature $T = 1$ eV [35]. The initial values of correlation length and magnetic field strength, ξ_0 and B_0 , at the temperature of magnetogenesis T_* , together with the two scaling indices n_ξ and n_E , fully determine the large-scale magnetic field decay, and as a result, the final configuration of the magnetic field.

Phenomenological arguments as well as numerical simulations show that $n_\xi = 1/2$ and $n_E = -1/2$ in the nonhelical case, while $n_\xi = 2/3$ and $n_E = -1/3$ in the helical case during the turbulent regime. The speed of growth of ξ_M is constant, independently of the relation between ξ_M and ξ_d . This implies that, in the case in which the initial correlation length of the magnetic field is comparable to the size of the cosmological horizon at the epoch of magnetogenesis, the final correlation length reaches 2×10^{-4} Mpc and 6×10^{-3} Mpc for nonhelical magnetic fields generated at EWPT and QCDPT, respectively. In the helical case, the correlation length reaches 10 kpc for fields generated at the QCDPT and 0.1 Mpc for the EWPT.

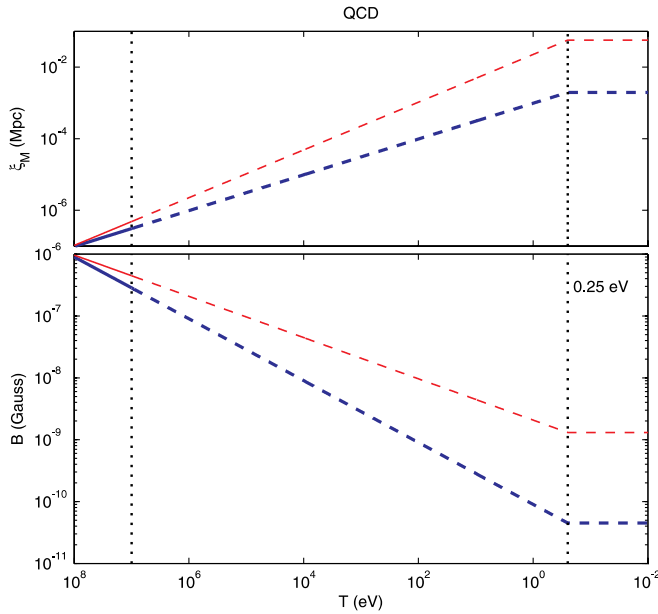


FIG. 5 (color online). The correlation length ξ_M (top panel) and the maximal allowed B_{\max} (bottom panel) for primordial helical (thin red) and nonhelical (thick blue) magnetic fields generated during QCDPT. Constraints on the magnetic field at $T = 0.25$ eV are set to $B_{\max} = 4.5 \times 10^{-11}$ G ($\xi_M = 2 \times 10^{-3}$ Mpc) and $B_{\max} = 1.3 \times 10^{-9}$ G ($\xi_M = 5.6 \times 10^{-2}$ Mpc) for nonhelical and helical cases, respectively. Dashed lines show areas where damping processes may reduce ideal estimates.

The evolutionary paths of magnetic field strength and correlation length in time and in the B , ξ_M parameter space are shown in Figs. 5–7. In principle, the free turbulence decay periods in the early Universe are intermittent, with periods of viscously damped evolution [32]. So, starting from 10 MeV, Figs. 5 and 6 show only maximal values of helical and nonhelical magnetic fields and their correlation lengths from QCD and electroweak phase transitions without accounting for any possible damping processes that can affect the given scaling laws. These maximal values are derived using several assumptions: the magnetic correlation length during phase transition matches the bubble size, and magnetic fields are excited with maximal amplitudes allowed by the BBN limit. In fact, before neutrino decoupling the viscous damping force \mathbf{f}_{visc} in Eq. (14) grows as $\nu \sim l_{\text{mfp},\nu} \sim \eta^4$, where $l_{\text{mfp},\nu}$ is the neutrino mean free path. This growth is much faster than the $\xi_M \sim \eta^{1/2}$ growth of the integral scale of the magnetic field. This means that, even if $\xi_M \gg l_{\text{mfp},\nu}$ at the moment of magnetogenesis, l_{mfp} catches up with ξ_M at a later time η_{visc} . Starting from this time and up to the moment of neutrino decoupling, the magnetic field stops to decay, $B \sim \text{const}$, because the fluid motions are damped by viscosity, $\nu \sim 0$, so that there is no coupling of the magnetic field to the fluid in this regime. However, turbulence restarts after the neutrino decoupling, so that the system returns to the same evolutionary track

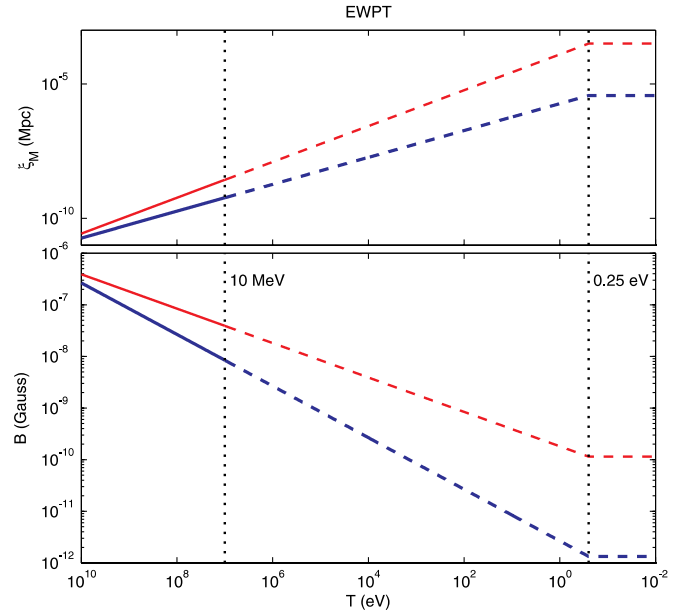


FIG. 6 (color online). The correlation length ξ_M (top panel) and the maximal allowed B_{\max} (bottom panel) for primordial helical (thin red) and nonhelical (thick blue) magnetic fields generated during EWPT. Constraints on the magnetic field at $T = 0.25$ eV are set to $B_{\max} = 1.3 \times 10^{-12}$ G ($\xi_M = 3.5 \times 10^{-6}$ Mpc) and $B_{\max} = 1.1 \times 10^{-10}$ G ($\xi_M = 3.1 \times 10^{-4}$ Mpc) for nonhelical and helical cases, respectively. Dashed lines show areas where damping processes may reduce ideal estimates.

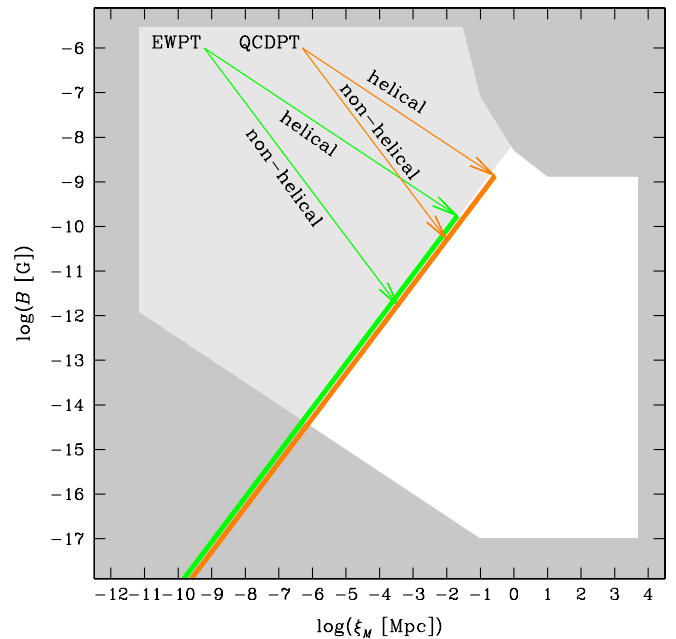


FIG. 7 (color online). Cosmological evolution of $B^{(\text{eff})}$ and ξ_M for magnetic fields generated at the EWPT (green) and QCDPT (orange). Arrows show the evolution of the strength and integral scale of helical and nonhelical fields during the radiation-dominated era up to their final values. Thick solid line(s) show the possible present-day strength and the integral scale of the phase-transition-generated magnetic fields.

shown in Fig. 7 just after neutrino decoupling. At lower temperatures, when the viscosity is provided by photon streaming, the viscous damping scale grows as $\nu \sim l_{\text{mfp},\gamma} \sim \eta^2$, where $l_{\text{mfp},\gamma}$ is the photon mean free path. In this time interval, the growth of ν is again faster than the growth of ξ_M , so that the episode of viscously damped evolution repeats when $l_{\text{mfp},\gamma}$ reaches ξ_M . This could again delay the advance of (B, ξ_B) along the evolutionary track shown in Fig. 7. The end point of the evolutionary track at the end of the radiation-dominated era is well defined by the condition that the correlation length of the magnetic field should not be shorter than the Silk damping scale times the Alfvén velocity [47]. The loci of the possible end points of the evolution are shown by the inclined thick solid (green/orange) lines in Fig. 7.

V. CONCLUSION

Our study shows that magnetic fields generated during phase transitions are comparable with the observational lower bound even if we account for large-scale decay as well as additional Alfvén wave-induced damping. The extremely low values of the smoothed magnetic field [24] do not imply that the effective magnetic field in the range 1 pc–1 kpc is small enough to result in observational changes in blazar emission spectra. The advantage of using the effective magnetic field lies in its independence of the spectral shape. In summary, if the magnetic field has been

generated during a phase transition, its correlation length is strongly limited. If future observations were to detect a weak magnetic field $\leq 10^{-14}$ – 10^{-15} G with a typical correlation length of the order of a few pc, this could serve as an indication of magnetogenesis during EWPT, while a somewhat stronger field with a correlation length of the order of kpc might indicate the presence of QCDPT magnetogenesis.

ACKNOWLEDGMENTS

We acknowledge fruitful discussions with R. Durrer. We appreciate helpful comments from L. Campanelli, K. Jedamzik, A. Kosowsky, and B. Ratra. We acknowledge partial support of computing resources provided by the Swedish National Allocations Committee at the Center for Parallel Computers at the Royal Institute of Technology in Stockholm and the Carnegie Mellon University supercomputer center. We acknowledge partial support from Swiss National Science Foundation SCOPES Grant No. 128040, NSF Grant No. AST1109180, and NASA Astrophysics Theory Program Grant No. NNX10AC85G. This work was supported in part by the European Research Council under AstroDyn Research Project No. 227952 and Swedish Research Council Grant No. 621-2007-4064. T. K. acknowledges the ICTP associate membership program. A. B. and A. G. T. acknowledge the McWilliams Center for Cosmology for hospitality.

-
- [1] L. M. Widrow, *Rev. Mod. Phys.* **74**, 775 (2002).
 - [2] J. P. Vallée, *New Astron. Rev.* **48**, 763 (2004).
 - [3] R. Beck, *AIP Conf. Proc.* **1085**, 83 (2008).
 - [4] M. J. Rees, Q. J. R. *Astron. Soc.* **28**, 197 (1987); K. Subramanian, D. Narasimha, and S. M. Chitre, *Mon. Not. R. Astron. Soc.* **271**, 15 (1994); R. M. Kulsrud and E. G. Zweibel, *Rep. Prog. Phys.* **71**, 046901 (2008).
 - [5] A. Kandus, K. E. Kunze, and C. G. Tsagas, *Phys. Rep.* **505**, 1 (2011).
 - [6] R. Beck, A. Brandenburg, D. Moss, A. Shukurov, and D. Sokoloff, *Annu. Rev. Astron. Astrophys.* **34**, 155 (1996).
 - [7] L. M. Widrow, D. Ryu, D. Schleicher, K. Subramanian, C. G. Tsagas, and R. A. Treumann, *Space Sci. Rev.* **166**, 37 (2012); D. Ryu, D. R. G. Schleicher, R. A. Treumann, C. G. Tsagas, and L. M. Widrow, *Space Sci. Rev.* **166**, 1 (2012).
 - [8] D. Grasso and H. R. Rubinstein, *Phys. Lett. B* **379**, 73 (1996).
 - [9] T. Kahniashvili, A. G. Tevzadze, S. K. Sethi, K. Pandey, and B. Ratra, *Phys. Rev. D* **82**, 083005 (2010); J. R. Shaw and A. Lewis, *Phys. Rev. D* **86**, 043510 (2012).
 - [10] A. Neronov and I. Vovk, *Science* **328**, 73 (2010); A. M. Taylor, I. Vovk, and A. Neronov, *Astron. Astrophys.* **529**, A144 (2011); I. Vovk, A. M. Taylor, D. Semikoz, and A. Neronov, *Astrophys. J.* **747**, L14 (2012).
 - [11] F. Tavecchio *et al.*, *Mon. Not. R. Astron. Soc.* **406**, L70 (2010); F. Tavecchio, G. Ghisellini, G. Bonnoli, and L. Foschini, *Mon. Not. R. Astron. Soc.* **414**, 3566 (2011); H. Huan and T. Weisgarber, [arXiv:1109.2863](https://arxiv.org/abs/1109.2863).
 - [12] K. Dolag, M. Kachelriess, S. Ostapchenko, and R. Tomas, *Astrophys. J.* **727**, L4 (2011).
 - [13] C. D. Dermer, M. Cavaldini, S. Razzaque, J. D. Finke, J. Chiang, and B. Lott, *Astrophys. J.* **733**, L21 (2011).
 - [14] T. C. Arlen, V. V. Vassiliev, T. Weisgarber, S. P. Wakely, and S. Y. Shafi, [arXiv:1210.2802](https://arxiv.org/abs/1210.2802).
 - [15] E. R. Harrison, *Mon. Not. R. Astron. Soc.* **147**, 279 (1970); T. Vachaspati, *Phys. Lett. B* **265**, 258 (1991); J. M. Cornwall, *Phys. Rev. D* **56**, 6146 (1997); G. Sigl, A. V. Olinto, and K. Jedamzik, *Phys. Rev. D* **55**, 4582 (1997); M. Joyce and M. E. Shaposhnikov, *Phys. Rev. Lett.* **79**, 1193 (1997); M. Hindmarsh and A. Everett, *Phys. Rev. D* **58**, 103505 (1998); K. Enqvist, *Int. J. Mod. Phys. D* **07**, 331 (1998); J. Ahonen and K. Enqvist, *Phys. Rev. D* **57**, 664 (1998); M. Giovannini, *Phys. Rev. D* **61**, 063004 (2000); T. Vachaspati, *Phys. Rev. Lett.* **87**, 251302 (2001); A. D. Dolgov and D. Grasso, *Phys. Rev. Lett.* **88**, 011301 (2001); D. Grasso, *Nucl. Phys. B, Proc. Suppl.* **110**, 189 (2002); D. Boyanovsky, H. J. de Vega, and M. Simionato, *Phys. Rev. D* **67**, 023502 (2003); **67**,

- 123505 (2003); A. Diaz-Gil, J. Garcia-Bellido, M. Garcia Perez, and A. Gonzalez-Arroyo, *Phys. Rev. Lett.* **100**, 241301 (2008); T. Stevens, M. B. Johnson, L. S. Kisslinger, E. M. Henley, W.-Y. P. Hwang, and M. Burkardt, *Phys. Rev. D* **77**, 023501 (2008); E. M. Henley, M. B. Johnson, and L. S. Kisslinger, *Phys. Rev. D* **81**, 085035 (2010); F. R. Urban and A. R. Zhitnitsky, *Phys. Rev. D* **82**, 043524 (2010), and references therein.
- [16] A. Brandenburg, K. Enqvist, and P. Olesen, *Phys. Rev. D* **54**, 1291 (1996).
- [17] J. M. Cornwall, *Phys. Rev. D* **56**, 6146 (1997); M. Joyce and M. E. Shaposhnikov, *Phys. Rev. Lett.* **79**, 1193 (1997); R. Jackiw and S.-Y. Pi, *Phys. Rev. D* **61**, 105015 (2000); W. D. Garretson, G. B. Field, and S. M. Carroll, *Phys. Rev. D* **46**, 5346 (1992); G. B. Field and S. M. Carroll, *Phys. Rev. D* **62**, 103008 (2000); M. Giovannini, *Phys. Rev. D* **61**, 063004 (2000); T. Vachaspati, *Phys. Rev. Lett.* **87**, 251302 (2001); L. S. Kisslinger, *Phys. Rev. D* **68**, 043516 (2003); D.-S. Lee, W. Lee, and K.-W. Ng, *Phys. Lett. B* **542**, 1 (2002); M. Laine, *J. High Energy Phys.* **10** (2005) 056; L. Campanelli and M. Giannotti, *Phys. Rev. D* **72**, 123001 (2005); V. B. Semikoz and D. D. Sokoloff, *Int. J. Mod. Phys. D* **14**, 1839 (2005); A. Diaz-Gil, J. Garcia-Bellido, M. Garcia Perez, and A. Gonzalez-Arroyo, *Phys. Rev. Lett.* **100**, 241301 (2008); C. J. Copi, F. Ferrer, T. Vachaspati, and A. Achúcarro, *Phys. Rev. Lett.* **101**, 171302 (2008); L. Campanelli, P. Cea, and G. L. Fogli, *Phys. Lett. B* **680**, 125 (2009); F. R. Urban and A. R. Zhitnitsky, *Phys. Rev. D* **82**, 043524 (2010); D. E. Kharzeev, *J. Phys. G* **38**, 124061 (2011).
- [18] T. Kahniashvili, A. G. Tevzadze, and B. Ratra, *Astrophys. J.* **726**, 78 (2011).
- [19] A. Boyarsky, J. Froelich, and O. Ruchayskiy, *Phys. Rev. Lett.* **108**, 031301 (2012).
- [20] C. J. Hogan, *Phys. Rev. Lett.* **51**, 1488 (1983).
- [21] R. Durrer and C. Caprini, *J. Cosmol. Astropart. Phys.* **11** (2003) 010.
- [22] A. S. Monin and A. M. Yaglom, *Statistical Fluid Mechanics* (MIT Press, Cambridge, MA, 1975).
- [23] M. Giovannini, *Lect. Notes Phys.* **737**, 863 (2008).
- [24] C. Caprini and R. Durrer, *Phys. Rev. D* **65**, 023517 (2001).
- [25] B. Ratra, *Astrophys. J.* **391**, L1 (1992).
- [26] C. Caprini, R. Durrer, and T. Kahniashvili, *Phys. Rev. D* **69**, 063006 (2004).
- [27] M. Christensson, M. Hindmarsh, and A. Brandenburg, *Phys. Rev. E* **64**, 056405 (2001).
- [28] D. T. Son, *Phys. Rev. D* **59**, 063008 (1999).
- [29] D. Biskamp, *Magnetohydrodynamic Turbulence* (Cambridge University Press, Cambridge, England, 2003).
- [30] D. Biskamp and W. C. Müller, *Phys. Rev. Lett.* **83**, 2195 (1999); *Phys. Plasmas* **7**, 4889 (2000).
- [31] L. Campanelli, *Phys. Rev. D* **70**, 083009 (2004).
- [32] R. Banerjee and K. Jedamzik, *Phys. Rev. D* **70**, 123003 (2004).
- [33] L. Campanelli, *Phys. Rev. Lett.* **98**, 251302 (2007).
- [34] T. Kahniashvili, A. Brandenburg, A. G. Tevzadze, and B. Ratra, *Phys. Rev. D* **81**, 123002 (2010).
- [35] K. Jedamzik and G. Sigl, *Phys. Rev. D* **83**, 103005 (2011).
- [36] P. A. Davidson, *Turbulence* (Oxford University Press, New York, 2004).
- [37] A. G. Tevzadze, L. Kisslinger, A. Brandenburg, and T. Kahniashvili, *Astrophys. J.* **759**, 54 (2012).
- [38] A. Saveliev, K. Jedamzik, and G. Sigl, *Phys. Rev. D* **86**, 103010 (2012).
- [39] T. Kahniashvili, A. Brandenburg, L. Campanelli, B. Ratra, and A. G. Tevzadze, *Phys. Rev. D* **86**, 103005 (2012).
- [40] D. Biskamp, *Nonlinear Magnetohydrodynamics* (Cambridge University Press, Cambridge, England, 2000).
- [41] P. Goldreich and S. Sridhar, *Astrophys. J.* **438**, 763 (1995).
- [42] A. Brandenburg, T. Kahniashvili, and A. Tevzadze (to be published).
- [43] C. Caprini, R. Durrer, and G. Servant, *J. Cosmol. Astropart. Phys.* **12** (2009) 024.
- [44] <http://pencil-code.googlecode.com/>.
- [45] M.-M. Mac Low, R. S. Klessen, and A. Burkert, *Phys. Rev. Lett.* **80**, 2754 (1998).
- [46] D. Biskamp and W.-C. Müller, *Phys. Rev. Lett.* **83**, 2195 (1999).
- [47] K. Jedamzik, V. Katalinic, and A. V. Olinto, *Phys. Rev. D* **57**, 3264 (1998); K. Subramanian and J. D. Barrow, *Phys. Rev. D* **58**, 083502 (1998); A. Mack, T. Kahniashvili, and A. Kosowsky, *Phys. Rev. D* **65**, 123004 (2002).